

## RXTE ALL-SKY MONITOR LOCALIZATION OF SGR 1627-41

DONALD A. SMITH<sup>1</sup>, HALE V. BRADT<sup>1</sup>, AND ALAN M. LEVINE<sup>1</sup>

### ABSTRACT

The fourth unambiguously identified Soft Gamma Repeater (SGR), SGR 1627-41, was discovered with the BATSE instrument on 1998 June 15 (Kouveliotou et al. 1998). Interplanetary Network (IPN) measurements and BATSE data constrained the location of this new SGR to a  $6^\circ$  segment of a narrow ( $19''$ ) annulus (Hurley et al. 1999a; Woods et al. 1998). We present two bursts from this source observed by the All-Sky Monitor (ASM) on *RXTE*. We use the ASM data to further constrain the source location to a  $5'$  long segment of the BATSE/IPN error box. The ASM/IPN error box lies within  $0.3'$  of the supernova remnant (SNR) G337.0-0.1. The probability that a SNR would fall so close to the error box purely by chance is  $\sim 5\%$ .

*Subject headings:* gamma rays: bursts – X-rays: bursts – stars: neutron

### 1. INTRODUCTION

The soft gamma repeaters (SGRs) were first identified as a separate class from “classical” gamma-ray bursts over ten years ago (Atteia et al. 1987; Kouveliotou et al. 1987; Laros et al. 1987). To date, four SGRs have been unambiguously identified. Attempts have been made to associate all these sources with supernova remnants (SNR). The location of SGR 0525-66 is consistent with the SNR N49 (Cline et al. 1982), and SGR 1806-20 has been associated with the SNR G10.0-0.3 (Kulkarni & Frail 1993; Kouveliotou et al. 1994; Kulkarni et al. 1994; Murakami et al. 1994). SGR 1900+14 has recently been localized to an error box of  $1.6$  square arcminutes, which lies just outside SNR G42.6+06 (Hurley et al. 1999b).

SGR 1627-41 was discovered with the BATSE instrument on 1998 June 15; a coarse location was promptly announced (Kouveliotou et al. 1998). Three days later, Hurley & Kouveliotou (1998) reported, based on data from GRB detectors in the Interplanetary Network (IPN), that the burst source was located within an annulus  $6'$  in width. Further analysis reduced the width of the annulus to  $19''$  (Hurley et al. 1999a). Earth limb considerations during bursts observed with BATSE restricted the burst source location along the IPN annulus to declinations between  $-43^\circ$  and  $-49^\circ$  (Woods et al. 1998). These localizations are all displayed in Figure 1. Woods et al. (1998) noted that the non-thermal core of the CTB 33 complex lay within this region. This core was identified as SNR G337.0-0.1 by Sarma et al. (1997), who estimated its distance to be  $11.0 \pm 0.3$  kpc. In response to the discovery of SGR 1627-41, this SNR was observed with the *BeppoSAX* Narrow Field Instruments. In this observation, a faint X-ray source was discovered at a location consistent with the IPN annulus, on the west side of G337.0-0.1 (Woods et al. 1999).

In this paper, we use observations by the *Rossi X-ray Timing Explorer* All-Sky Monitor of two bursts from SGR 1627-41 to constrain the source’s position along the IPN annulus, and we discuss the possible association of SGR 1627-41 with the SNR G337.0-0.1.

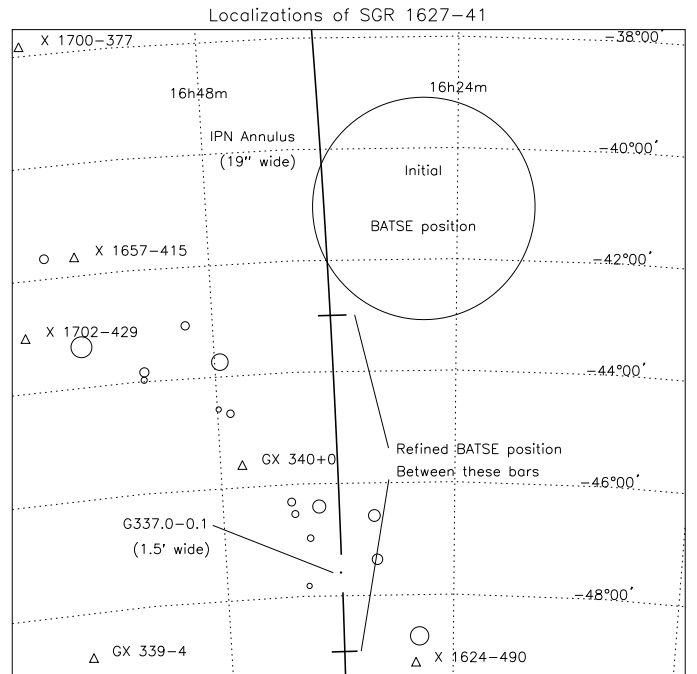


Fig. 1 – Localizations of SGR 1627-41. Known X-ray sources in the ASM catalog with typical brightnesses above  $\sim 50$  mCrab are plotted as triangles. SNRs from the Green catalog are plotted as circles with diameters equal to the mean angular size listed in the catalog. The IPN annulus is not plotted near the SNR G337.0-0.1 to avoid obscuring the  $1.5'$  circle.

### 2. INSTRUMENT

The ASM consists of three Scanning Shadow Cameras (SSCs) mounted on a motorized rotation drive. Each SSC contains a proportional counter with eight resistive anodes that are used to obtain a one-dimensional position along the direction parallel to the anodes for each detected event. The proportional counter views a  $12^\circ \times 110^\circ$  (FWZI) field through a random-slit mask. The mask consists of six unique patterns, oriented such that the

<sup>1</sup>Center for Space Research and Department of Physics, MIT, Cambridge, MA 02139

slits run perpendicular to the anodes.

The intensities of known sources in the field of view (FOV) are derived via a fit of model slit-mask shadow patterns to histograms of counts as a function of position in the detector. Normally, the residuals from a successful fit in the 1.5–12 keV band are then cross-correlated with each of the expected shadow patterns corresponding to a set of possible source directions which make up a grid covering the FOV. A peak in the resulting cross-correlation map indicates the possible presence and approximate location of a new, uncataloged X-ray source (Levine et al. 1996).

In addition to “position” data products, time-series data on the total number of counts registered in each SSC are recorded in 1/8 s bins. The position of each count in the detector is not preserved in the time-series mode.

### 3. OBSERVATIONS AND ANALYSIS

Two bursts were detected in SSC 3 of the ASM on 1998 June 17.943917 and 17.954243 (UTC). The time histories of these bursts are shown in Figure 2. Each burst was short ( $\lesssim 2$  s), bright (5–12 keV fluxes of  $\sim 9$  and  $\sim 23$  Crab at peak), and hard (no significant flux below 5 keV), characteristic of SGR bursts. At these times, BATSE could not observe SGR 1627–41 due to Earth-occultation (C. Kouveliotou 1998, private communication), but SGR 1627–41 was known to be active around this time, and the BATSE and IPN localizations of SGR 1627–41 were consistent with the FOV of the ASM at the times of these events. We therefore attribute these bursts to SGR 1627–41.

The energy spectra of bursts from SGR 1806–20 are known to drop rapidly below  $\sim 14$  keV (Fenimore, Laros, & Ulmer 1994), and this property seems consistent with the ASM observations of SGR 1627–41 reported here. These two bursts were not detected in the lowest two energy channels of the ASM (1.5–5 keV). We therefore performed the cross-correlation analysis using only the data from the highest energy channel (5–12 keV). We found significant peaks in each of the two cross-correlation maps. The celestial locations of these peaks are consistent with each other and with the refined BATSE/IPN position. The first burst detection has a statistical significance of  $4.3\sigma$ , while the second burst was detected with a significance of  $5.7\sigma$ . These levels of significance do not take the number of trials in the search into account.

Since there are roughly 10000 independent position bins in the FOV of an SSC, the probability of measuring a noise peak of at least  $4.3\sigma$  somewhere in the FOV is roughly 0.08, and the probability of measuring a  $5.7\sigma$  peak or higher is roughly  $10^{-3}$ . There are roughly 60 independent position bins within the refined BATSE/IPN error box. The probability that both peaks would fall at random in the same location and that the common location should overlap the BATSE/IPN error box is  $60 \times (10^{-4})^2 \sim 10^{-6}$ . We are therefore confident that these peaks do represent detections of SGR 1627–41.

To refine the source position, we determined which regions of the IPN annulus were consistent with the ASM observations of the two bursts. At the time of the first burst, the FOV of SSC 3 did not cover positions along the annulus north of  $-45^\circ$ , while at the time of the second burst, the FOV did not cover positions along the annulus south of  $-50.6^\circ$ . We ran multiple trials of our ASM shadow-pattern fitting program for the 5–12 keV data from each of the two 90 s observations. In each trial, a source was assumed to be at one of 1600 locations along the center line of the segment of the IPN annulus with  $-50^\circ \leq \delta \leq -45^\circ$ .

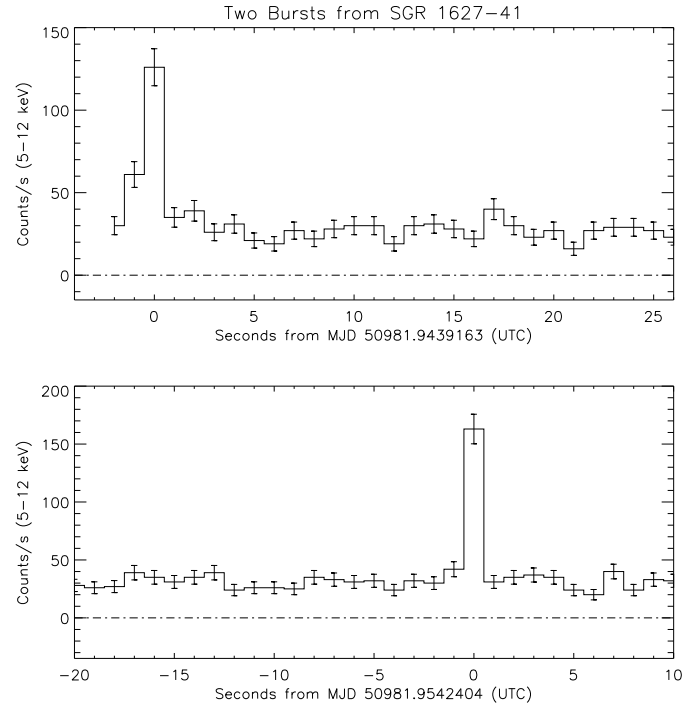


Fig. 2 – Counts per 1-s bin around the times of two bursts from SGR 1627–41, as observed between 5–12 keV by SSC 3. The count rate includes contributions from all X-ray sources in the FOV, as well as the diffuse X-ray background. No background subtraction has been performed.

Each trial yields the fitted intensity of the source as well as a  $\chi^2$  goodness of fit statistic. For both observations, the best fit was found to be near  $\delta = -47.6^\circ$  (Fig. 3).

For each of the two ASM observations, regions for which  $\chi^2 < \chi^2_{\min} + 2.7, 4.0$ , or  $6.6$  yielded 90%, 95%, or 99% confidence intervals, respectively, for the source declination. These intervals are presumed to reflect counting statistics. We estimated the effect of systematic errors by projecting the measured magnitude of the position error for strong sources onto the direction of the BATSE/IPN error box. This magnitude was measured by Smith et al. (1999) to be  $1.9'$  for 95% confidence intervals along the direction parallel to the proportional counter anodes. We added  $1.9'/\cos\theta$  in quadrature with the errors estimated from the  $\chi^2$  values, where  $\theta$ , the angle between the IPN annulus and the anode direction, was  $7^\circ$  for the first burst and  $43^\circ$  for the second burst.

We thus derive two independent measurements of the declination of SGR 1627–41 along the IPN annulus:  $\delta_1 = -47^\circ.603^{+0.053}_{-0.051}$  and  $\delta_2 = -47^\circ.640^{+0.091}_{-0.096}$  at 95% confidence. We find a joint error box of  $\delta = -47^\circ.621 \pm 0.045$  (J2000) by taking the weighted average of the two measurements. We calculate similar intervals for 90% and 99% confidence levels, using the same value for the systematic error. These three intervals are  $4.9', 5.4'$ , and  $6.3'$  long, in order of increasing confidence. All three intervals are plotted as dark bars in Figure 3 and, together with the IPN annulus, as boxes in Figure 4. The center of these boxes lies  $0.13^\circ$  below the galactic plane. These boxes are consistent with the  $1'$  location of the persistent X-ray source localized by Woods et al. (1999), which is also plotted in Figure 4.

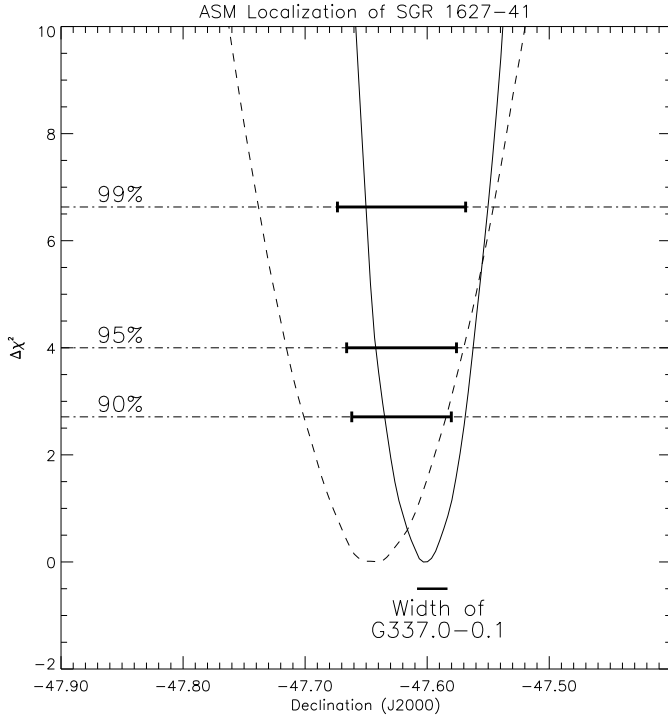


Fig. 3 – The change in  $\chi^2$  as a function of declination along the IPN annulus, relative to the minimum values. The results from the burst of June 17.943917 are graphed as a solid line, while those from June 17.954243 are graphed as a dashed line. The location and extent of G337.0–0.1 is indicated by the dark horizontal bar below the curves. The weighted average error box at each confidence level is indicated by a darkened interval.

Since the position of the source is well-constrained, the fits to the position data yield source intensities that can be used to estimate the number of counts actually detected from the source. Since there are no other known variable sources in the FOV, we can use the time-series data to estimate the peak flux of the bursts as well as investigate the possible presence of non-burst emission. Comparison of the count rates with the observed brightness of the Crab Nebula yields burst peak fluxes (1-s bins; 5–12 keV) of  $(1.1 \pm 0.2) \times 10^{-7}$  and  $(2.7 \pm 0.3) \times 10^{-7}$  erg cm $^{-2}$  s $^{-1}$ . These values may be underestimates because the burst spectrum is substantially harder than the Crab spectrum in this energy range. We find that, for both bursts, the number of counts derived from the position data is consistent with the number of counts detected in the bursts as recorded in the time-series data. This yields a weak upper limit of  $\sim 2 \times 10^{-8}$  erg cm $^{-2}$  s $^{-1}$  ( $3\sigma$ ) on any non-burst emission in the 1.5–12 keV band from the SGR during these observations.

A search for pulsations in the 5–12 keV time-series data was conducted by performing FFTs on 64 s of data after the burst events. In neither observation was any coherent signal between 0.015 and 4.000 Hz detected to an upper limit on the amplitude of  $\sim 2.4$  c/s at 95% confidence. At the position of the ASM/IPN error box, this limit corresponds to a peak-to-peak modulation of  $\sim 340$  mCrab.

#### 4. DISCUSSION

The  $19'' \times 4.9'$  ASM/IPN error box for the bursting source passes within  $1.05'$  of the center of SNR G337.0–0.1, which is

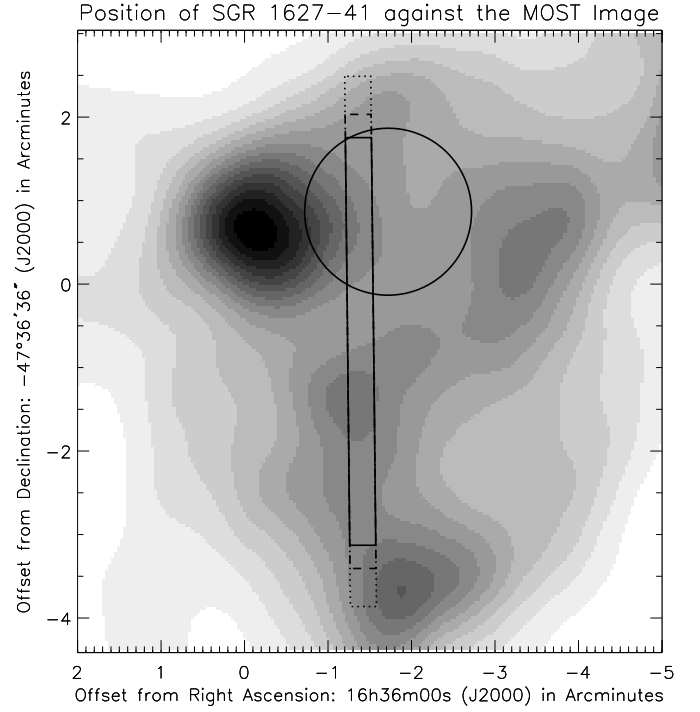


Fig. 4 – The joint ASM/IPN localization of the bursts from SGR 1627–41 is graphed over the MOST 0.8 GHz image (Whiteoak & Green, 1996) of SNR G337.0–0.1, the pronounced dark region. The width of the box is set by the IPN  $3\sigma$  error annulus. The lengths represent three confidence levels for the ASM localization: 99% (dotted line), 95% (dashed line), and 90% (solid line). Also plotted is the error circle for the location of the weak persistent source observed by *BeppoSAX*. (Woods et al. 1999).

a non-thermal shell,  $0.75'$  in mean radius, embedded in a complex HII region (Sarma et al. 1997). Since arguments have been made to associate each of the three previously known SGRs with nearby SNRs, it is tempting to conclude that SGR 1627–41 is a magnetar that was born in the same supernova explosion that produced SNR G337.0–0.1. However, this is a very crowded region of the sky. The *a posteriori* probability of finding a SNR near the error box for SGR 1627–41 cannot be discounted, and it has been argued (e.g., Gaensler & Johnston 1995) that the number of pulsar/SNR associations has been overestimated due to the underestimation of the chances of appearing close on the sky by geometric projection.

The north end of the ASM/IPN error box lies  $0.3'$  outside the nominal edge of G337.0–0.1. We estimate the probability of a chance association after the method of Kulkarni & Frail (1993). We inflate the size of all the SNRs in Green's catalog (1998) by  $0.3'$  and convolve them with the ASM/IPN error box for SGR 1627–41. The fraction of the sky covered by the total of all the resulting areas gives the probability of a chance association, if the distribution of SNRs is uniform. The ASM/IPN error box is less than  $0.1^\circ$  away from the galactic plane, and SNRs are strongly clustered along the galactic plane as well as toward the galactic center. We therefore apply the method by summing over the areas of the 19 SNRs in the region with galactic coordinates of  $327^\circ < \ell < 347^\circ$  and  $|b| < 0.5$ . We obtain a probability of 5.4% that the ASM/IPN error box would fall within  $0.3'$  of a SNR by chance.

Another method of evaluating the association between SGR 1627–41 and G337.0–0.1 is to consider the conditional probability of finding the SGR within the ASM error box given that it must be somewhere within the revised BATSE/IPN error box. The hypothesis that the SGR was born in the same explosion that created G337.0–0.1 gives us one model for the underlying probability distribution of the source location. We assume that the SGR has been traveling for  $10^4$  y from the center of G337.0–0.1 (assumed to be 11 kpc from Earth) at a velocity drawn from a three-dimensional Maxwellian distribution with an rms value of 500 km/s. We convert this three-dimensional distribution to a distribution on the sky (a two-dimensional Gaussian with a standard deviation of 1.6'), and renormalize this function by requiring that its integral over the BATSE/IPN error box be equal to unity. The integral of the resulting density function over the ASM 90% confidence error box yields a value of 0.749.

To evaluate a second model, we compute the probability of finding the SGR within the ASM error box if its location within the BATSE/IPN error box is drawn from a uniform distribution. Under that assumption, the probability is simply the ratio of the areas of the two error boxes, or 0.0136.

A comparison between these two probabilities indicates that the first hypothesis is a more reasonable explanation for the data than the second. This should not be taken as proof that the SGR actually did originate at the center of SNR G337.0–0.1, as it is also possible that the SGR may be associated with something other than G337.0–0.1 that belongs to a class of objects that clusters along the galactic plane.

An association between SGR 1627–41 and G337.0–0.1 does not require that unreasonable physical characteristics be attributed to the system. At an assumed distance of 11 kpc,

the ASM/IPN error box lies 4 pc away from the center of G337.0–0.1, projected onto the plane of the sky. G337.0–0.1 itself is 5.1 pc in diameter. The radius of a SNR in the Sedov-Taylor phase of its expansion is given by  $R = (31.5 \text{ pc})(E_{51}/n_0)^{1/5} t_5^{2/5}$  (Shull, Fesen, & Saken 1989). If we assume  $E_{51} \sim 1$ , then  $t_5 = n_0^{1/2} (R/31.5)^{5/2}$ . Since OH masers have been associated with this SNR (Frail et al. 1996), the local density must fall within the range  $(1 - 30) \times 10^4 \text{ cm}^{-3}$  (Lockett, Gauthier, & Elitzur 1999). This means the age of the remnant must fall between  $(2 - 10) \times 10^4$  y. These values are within an order of magnitude of the estimated age of magnetars,  $\sim 10,000$  y (Thompson & Duncan 1996), and they imply a projected velocity for the magnetar between 40 and 200 km/s. These are reasonable values for the projected velocity of a neutron star.

A distance of 11 kpc also does not demand an excessive energy budget for these bursts. Bursts from SGR 1806–20 have been observed to reach total peak luminosities of  $\sim 10^{42}$  erg/s, with a third of the emission above 30 keV (Fenimore et al. 1994). The two bursts detected by the ASM from SGR 1627–41, assuming isotropic emission from an 11 kpc distance, reach peak 5–12 keV luminosities of 2 and  $3 \times 10^{39}$  erg/s, only 0.1% of the above total.

We thank Kevin Hurley for providing the IPN annulus and Peter Woods for providing the *BeppoSAX* source location. DS wishes to thank Derek Fox, Bryan Gaensler and Vicky Kaspi for helpful discussions. Support for this work was provided in part by NASA Contract NAS5-30612. The MOST is operated by the University of Sydney with support from the Australian Research Council and the Science Foundation for Physics within the University of Sydney.

## REFERENCES

Atteia, J.-L., et al. 1987, *ApJ*, 320, L105  
 Cline, T., et al. 1982, *ApJ*, 255, L45  
 Fenimore, E., Laros, J., & Ulmer, A. 1994, *ApJ*, 432, 742  
 Frail, D., Goss, W., Reynoso, E., Giacani, E., Green, A., & Otrupcek, R. 1996, *AJ*, 111, 1651  
 Gaensler, B., & Johnston, S. 1995, *MNRAS*, 277, 1243  
 Green, D. 1998, <http://www.mrao.cam.ac.uk/surveys/snrs/>  
 Hurley, K., & Kouveliotou, C. 1998, *GCN Circ.* 110  
 Hurley, K., et al. 1999a, *ApJ*, submitted  
 Hurley, K., Kouveliotou, C., Woods, P., Cline, T., Butterworth, P., Mazets, E., Golenetskii, S., & Frederics, D. 1999b, *ApJ*, 510, L107  
 Kouveliotou, C., et al. 1987, *ApJ*, 332, L21  
 Kouveliotou, C., et al. 1994, *Nature*, 368, 125  
 Kouveliotou, C., Kippen, M., Woods, P., Richardson, G., & Connaughton, V. 1998, *GCN Circ.* 107  
 Kulkarni, S., & Frail, D. 1993, *Nature*, 365, 33  
 Kulkarni, S., Frail, D., Kassim, N., Murakami, T., & Vasisht, G. 1994, *Nature*, 368, 129  
 Laros, J., et al. 1987, *ApJ*, 320, L111  
 Levine, A., Bradt, H., Cui, W., Jernigan, J., Morgan, E., Remillard, R., Shirey, R., & Smith, D. 1996, *ApJ*, 469, L33  
 Lockett, P., Gauthier, E., & Elitzur, M. 1999, *ApJ*, 511, 235  
 Murakami, T., Tanaka, Y., Kulkarni, S., Ogasaka, Y., Sonobe, T., Ogawara, Y., Aoki, T., & Yoshida, A. 1994, *Nature*, 368, 127  
 Sarma, A., Goss, W., Green, A., & Frail, D. 1997, *ApJ*, 483, 335  
 Shull, J., Fesen, R., & Saken, J. 1989, *ApJ*, 346, 860  
 Smith, D., et al. 1999, *ApJ*, submitted  
 Thompson, C., & Duncan, R. 1996, *ApJ*, 473, 322  
 Whiteoak, J., & Green, A. 1996, *A&AS*, 118, 329–380  
 Woods, P., Kippen, M., van Paradijs, J., Kouveliotou, C., McCollough, M., & Hurley, K. 1998, *GCN Circ.* 113  
 Woods, P., et al. 1999, *ApJ*, submitted